Supplement of Biogeosciences, 23, 1809–1832, 2026
https://doi.org/10.5194/bg-23-1809-2026-supplement

Biogeosciences Open Access EGU

Supplement of

Evaluating glycerol dialkyl glycerol tetraether (GDGT)-based reconstructions from varved lake sediments during the Holocene

Ashley M. Abrook et al.

Correspondence to: Ashley M. Abrook (a.abrook@soton.ac.uk)

Supplementary Information

Evaluating glycerol dialkyl glycerol tetraether (GDGT)-based reconstructions from varved lake sediments during the Holocene.

Abrook et al.

S1. Additional LC-MS Analysis

The polar fraction was analysed by high-performance liquid chromatography (HPLC) mass spectrometry (MS) using an Agilent 1260 HPLC coupled to an Agilent 6130 single quadrupole MSD following the method. Normal phase separation was achieved using two HPLC columns (BEH HILIC columns, 2.1 x 150 mm, 1.7 µm) using n-hexane (solvent A) and n-hexane:isopropanol (IPA) 9:1 (v/v) (solvent B). Separation was achieved using 18% solvent B for 25 min, increasing to 35% over 25 mins, then 100% solvent B over 30 mins, for one minute before returning to 18% solvent B over 19 mins to equilibrate the column prior to the next injection at a flow rate of 2.0 µl min^{-1}.

Detection was achieved using positive ion APCI of the eluent. Conditions for the MS were set as: nebulizer pressure 60 psi, vaporizer temperature 400 °C, drying gas (N_2) flow 6 L/min and temperature 200°C, capillary voltage −3 kV, corona 5 µA (~3.2 kV) and a dwell time of 234 ms per ion (Hopmans et al., 2016).

GDGTs were detected using SIM and by mass scanning from m/z 950−1450 on the Agilent HPLC – MS (Hopmans et al., 2016). Relative GDGTs abundance was quantified by integration of the peak areas using Agilent ChemLabs software and via comparison to both internal marine and peat standards.

S2. Additional reconstructions

Full reconstructions of LST and brGDGT temperatures are given in S1 and S2. Where appropriate the uncertainty is provided. This is a calibration uncertainty of the Raberg et al. (2021) equation and a 95% uncertainty with the Bayesian approach of Martinez-sosa et al. (2021). Additionally, correlations are shown in S3 to S8 where statistically significant correlations exist between GDGT metrics and temperature or other lake process parameters. We also include here an f[CREN'] reconstruction, S9, from Nautajärvi and Meerfelder Maar.

For comparative purposes, we provide additional site information to aid in our interpretations from Diss Mere, Meerfelder Maar and Nautajärvi, S10, S11 and S12.

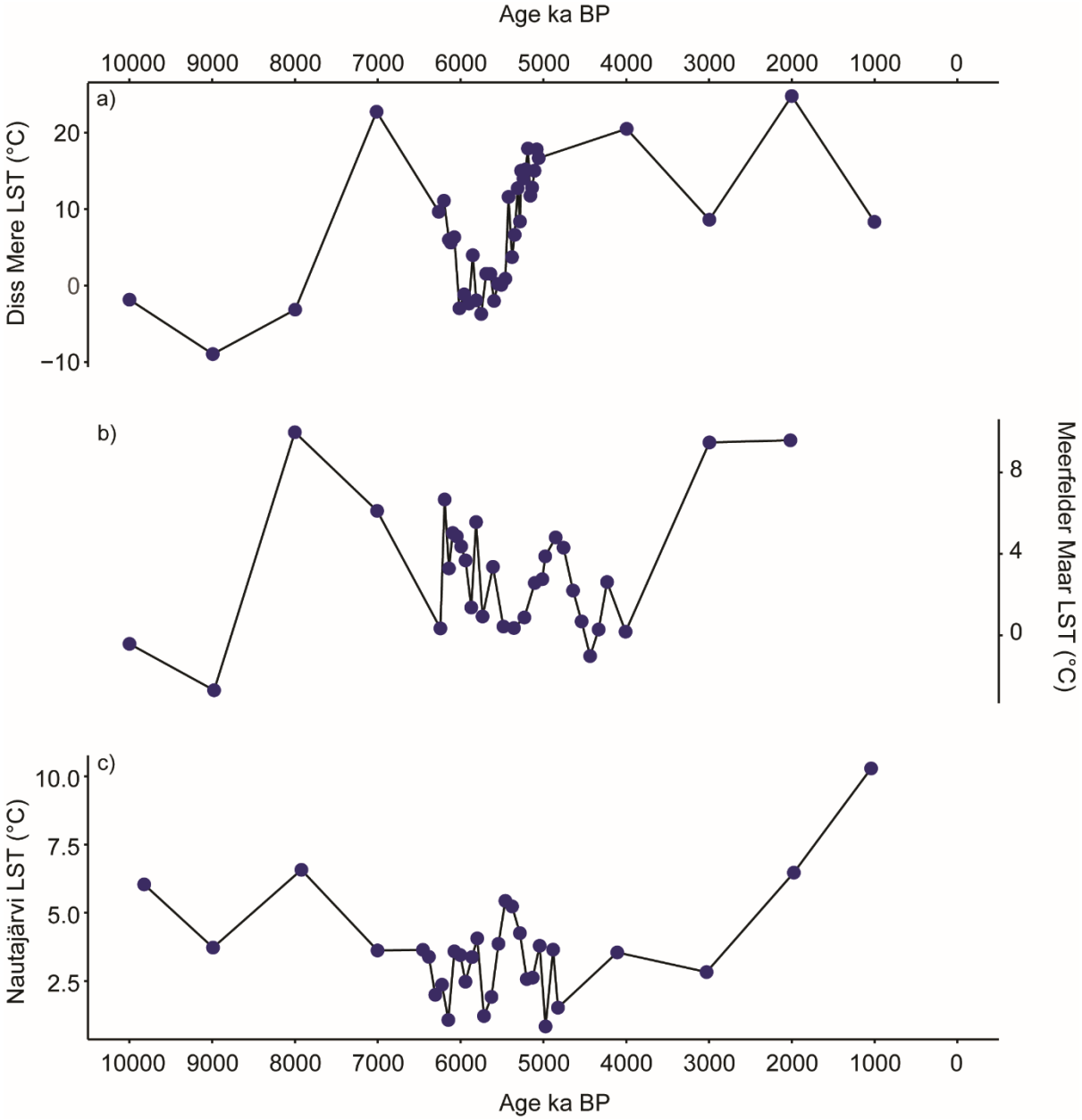

Figure S1. TEX_{86} reconstructed Lake Surface Temperature (LST) reconstructions from the three sites in this study a) Diss Mere, b) Meerfelder Maar, c) Nautajärvi.

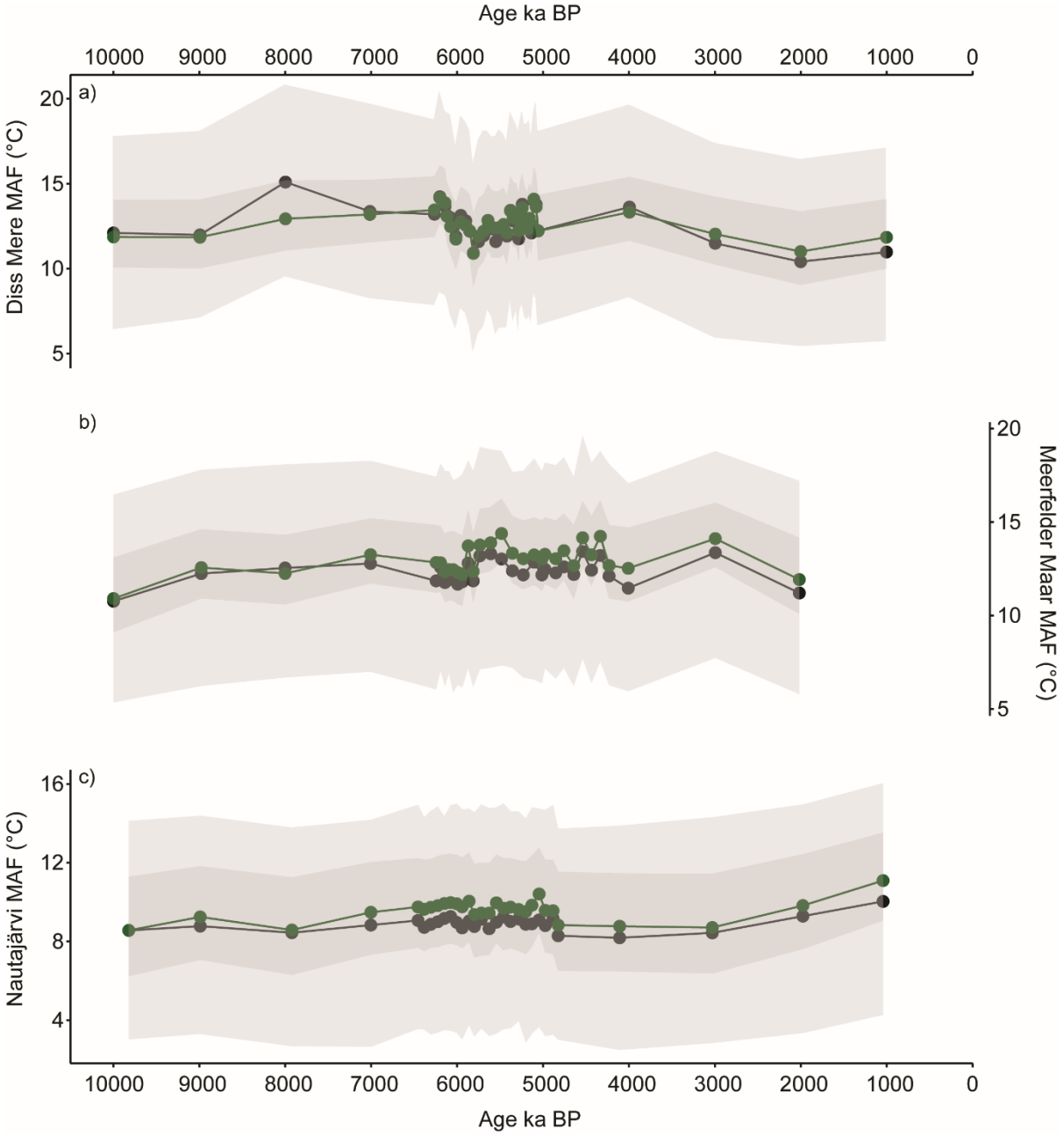

Figure S2. Mean Temperature of Months Above Freezing (MAF) reconstructions from each of the lake sites in this study: a) Diss Mere, b) Meerfelder Maar, and c) Nautajärvi. The two different reconstructions are black, Bayesian-based MAF reconstructions (Martinez-Sosa et al., 2021); and green, multivariate methylation set MAF reconstructions (Raberg et al., 2021). The dark grey error bars are txhe calibration uncertainty associated with Raberg et al. (2021). The light grey error bars represent the 95% confidence interval associated Martinez-Sosa et al. (2021).

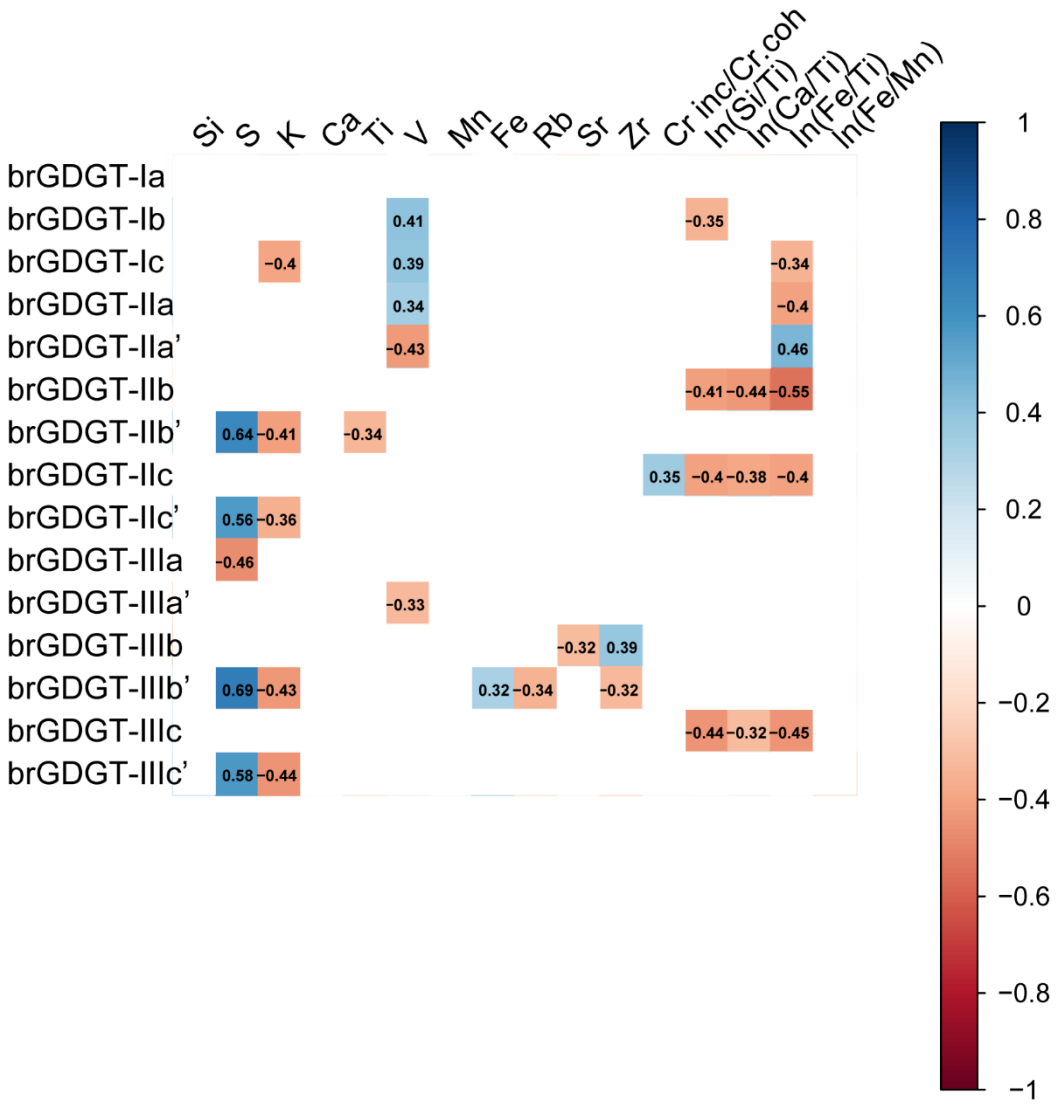

Figure S3. Pearson's correlation coefficients between identified GDGT compounds and µ-XRF data from Diss Mere. Shown are significant correlations only.

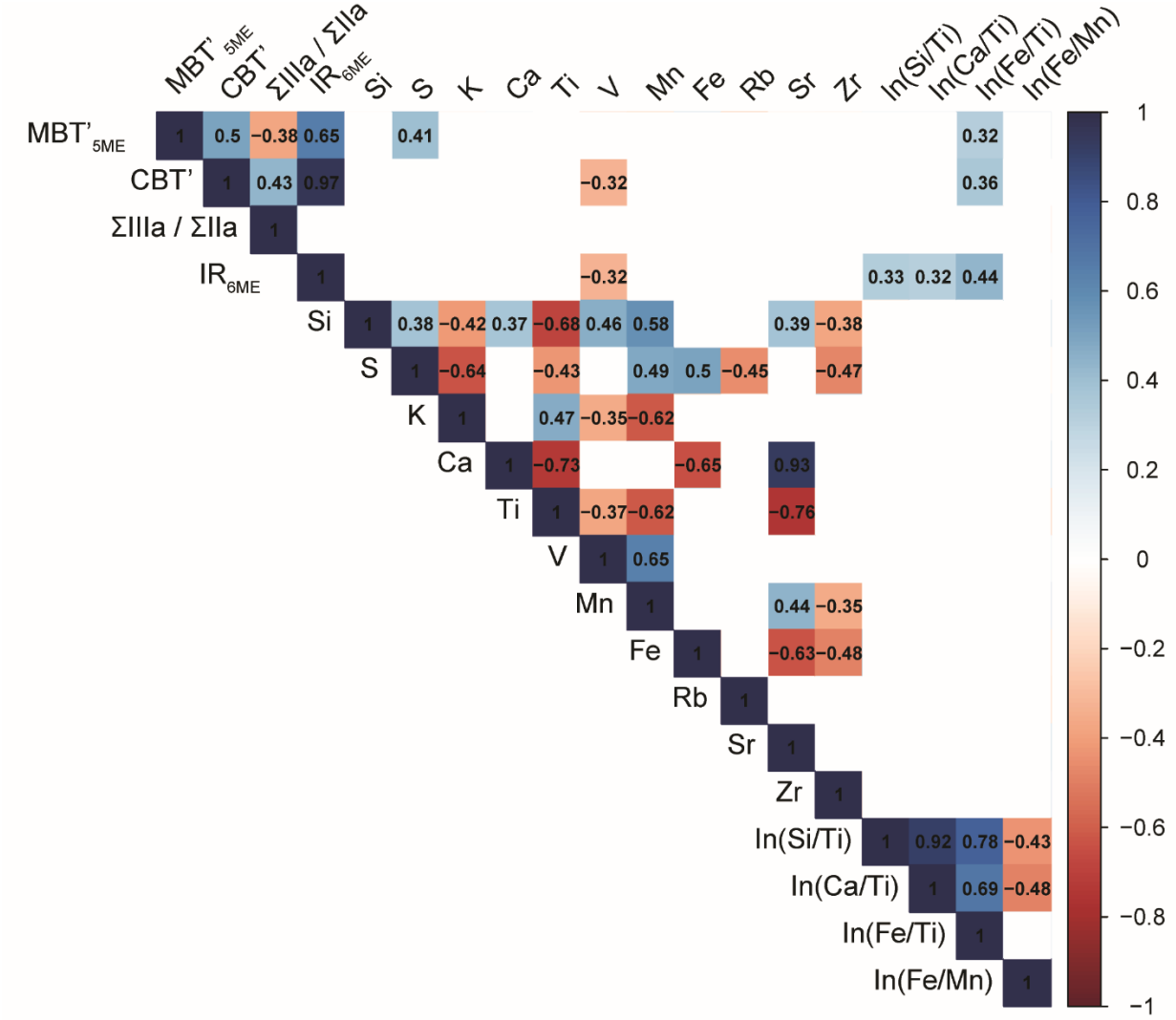

Figure S4. Pearson's correlation coefficients between the main GDGT metrics and μ-XRF data from Diss Mere. Shown are significant correlations only.

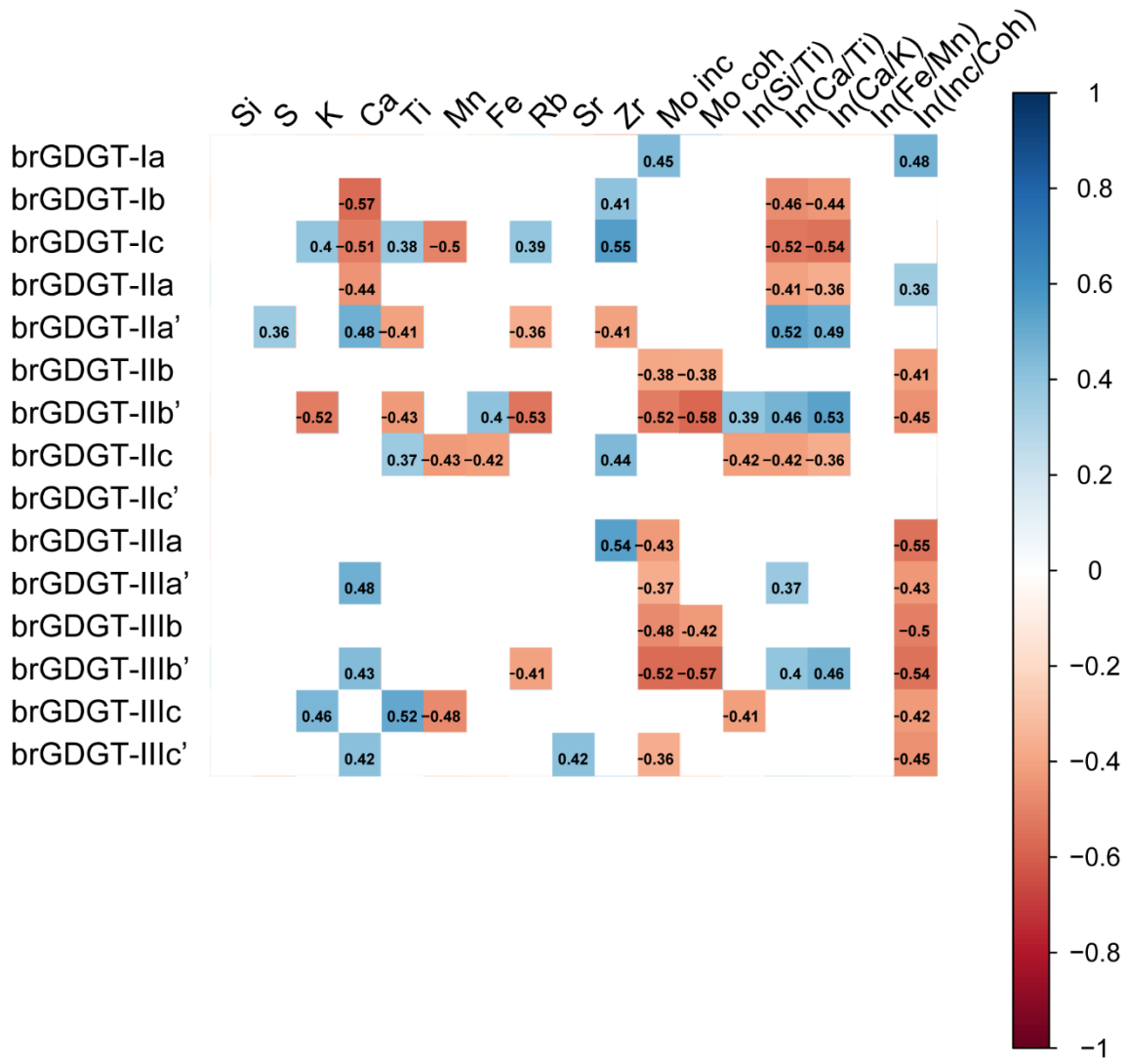

Figure S5. Pearson's correlation coefficients between identified GDGT compounds and µ-XRF data from Meerfelder Maar. Shown are significant correlations only.

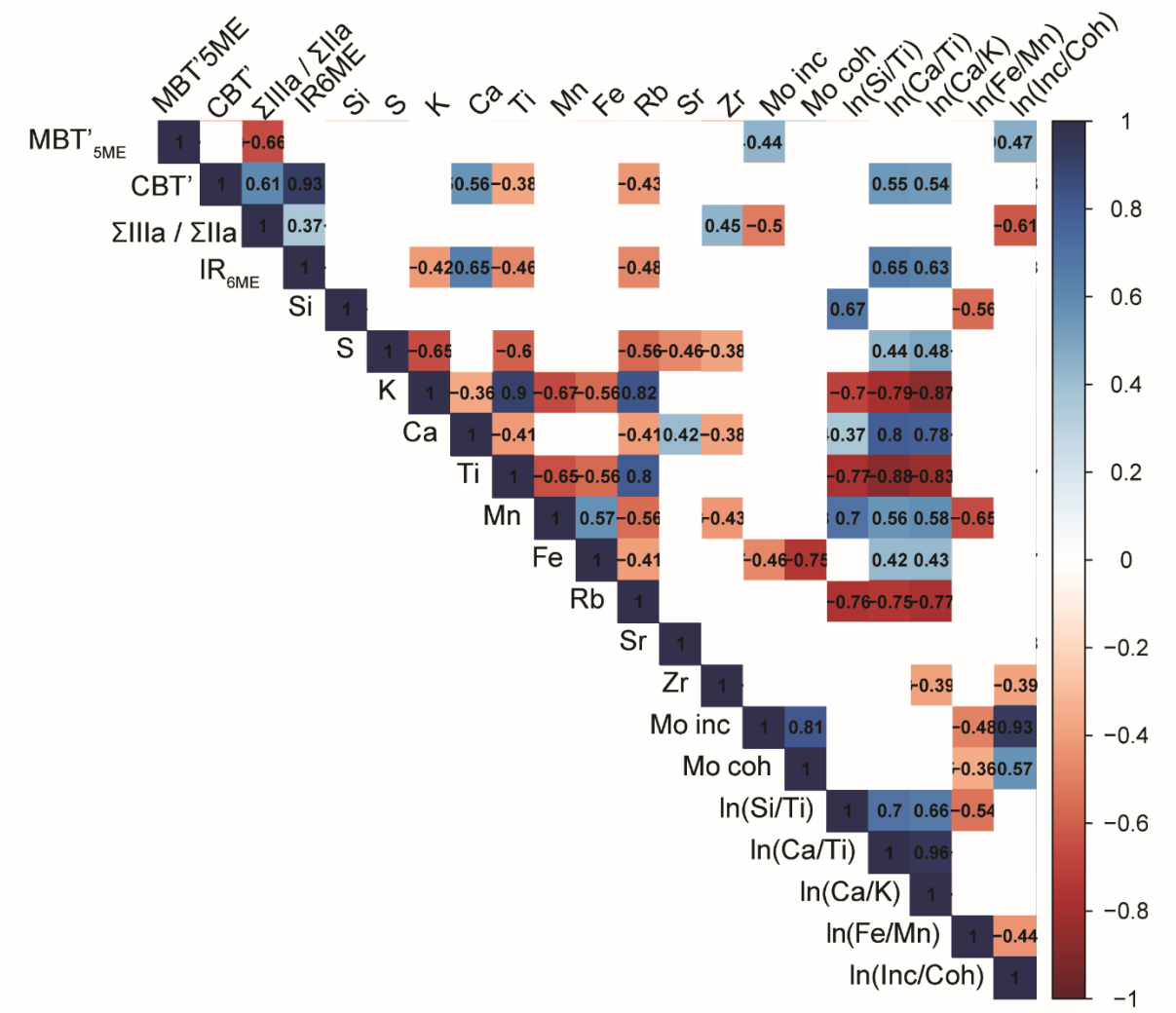

Figure S6. Pearson's correlation coefficients between the main GDGT metrics and μ-XRF data from Meerfelder Maar. Shown are significant correlations only.

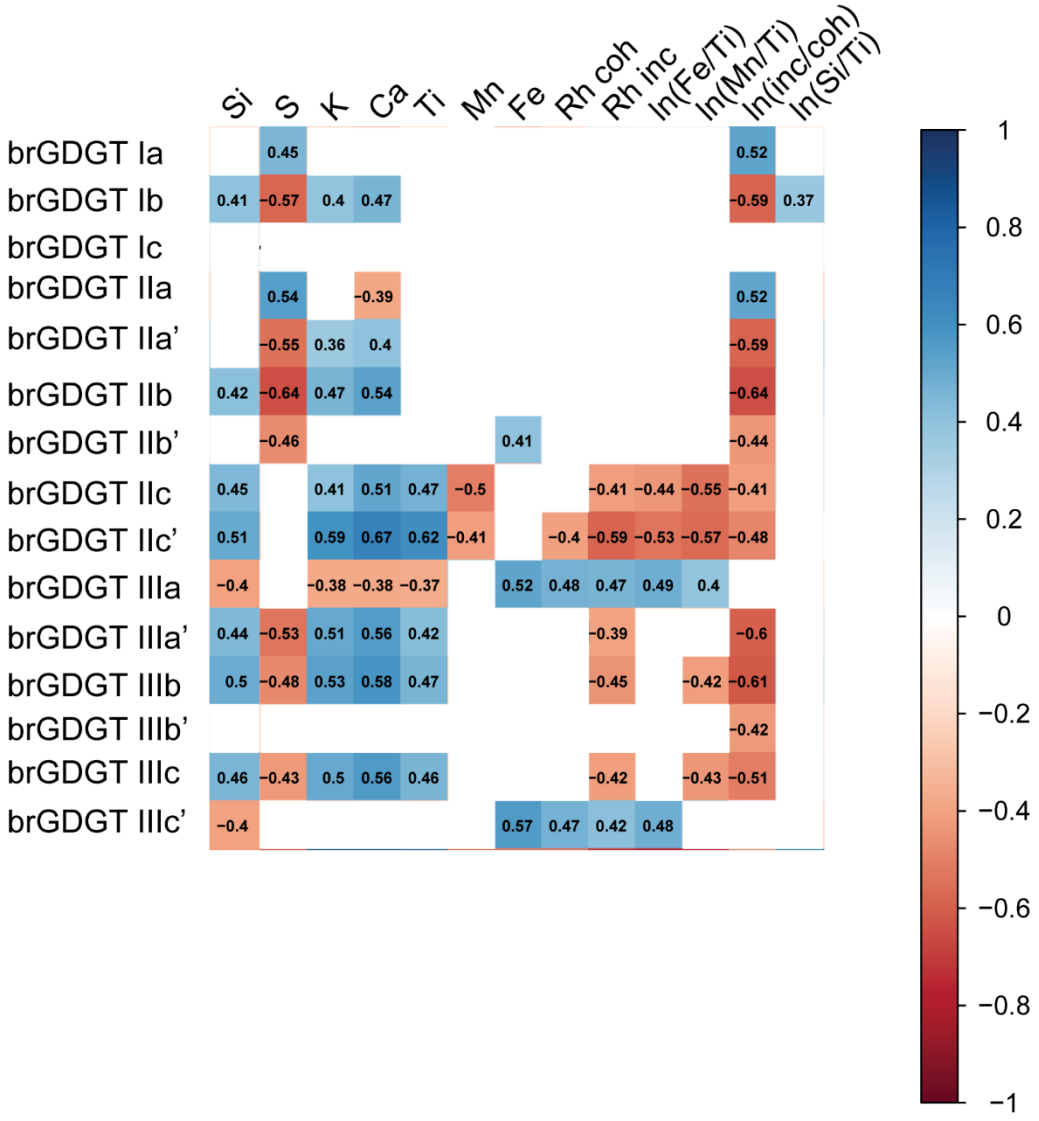

Figure S7. Pearson's correlation coefficients between identified GDGT compounds and μ-XRF data from Nautajärvi. Shown are significant correlations only.

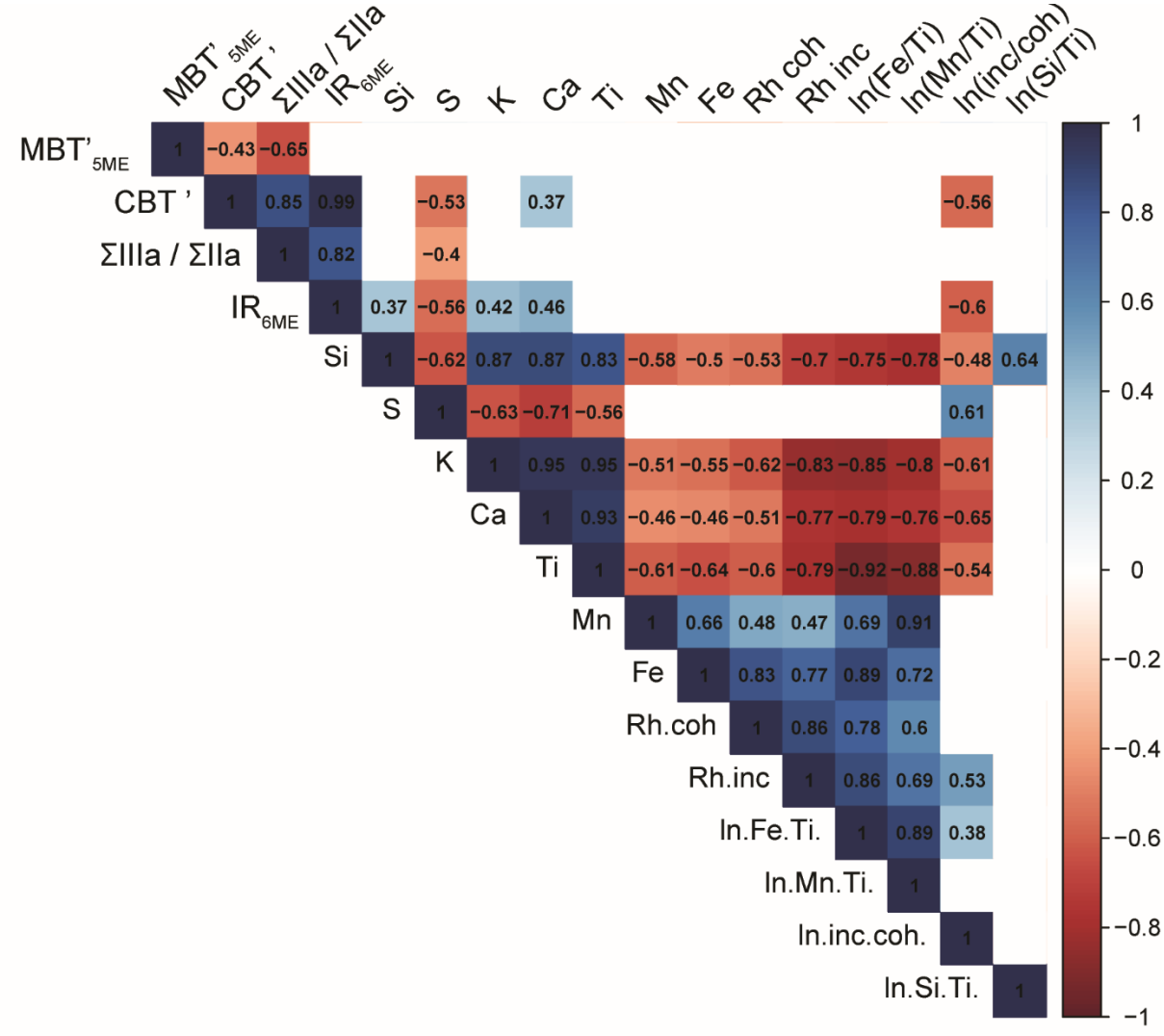

Figure S8. Pearson's correlation coefficients between the main GDGT metrics and μ-XRF data from Nautajärvi. Shown are significant correlations only.

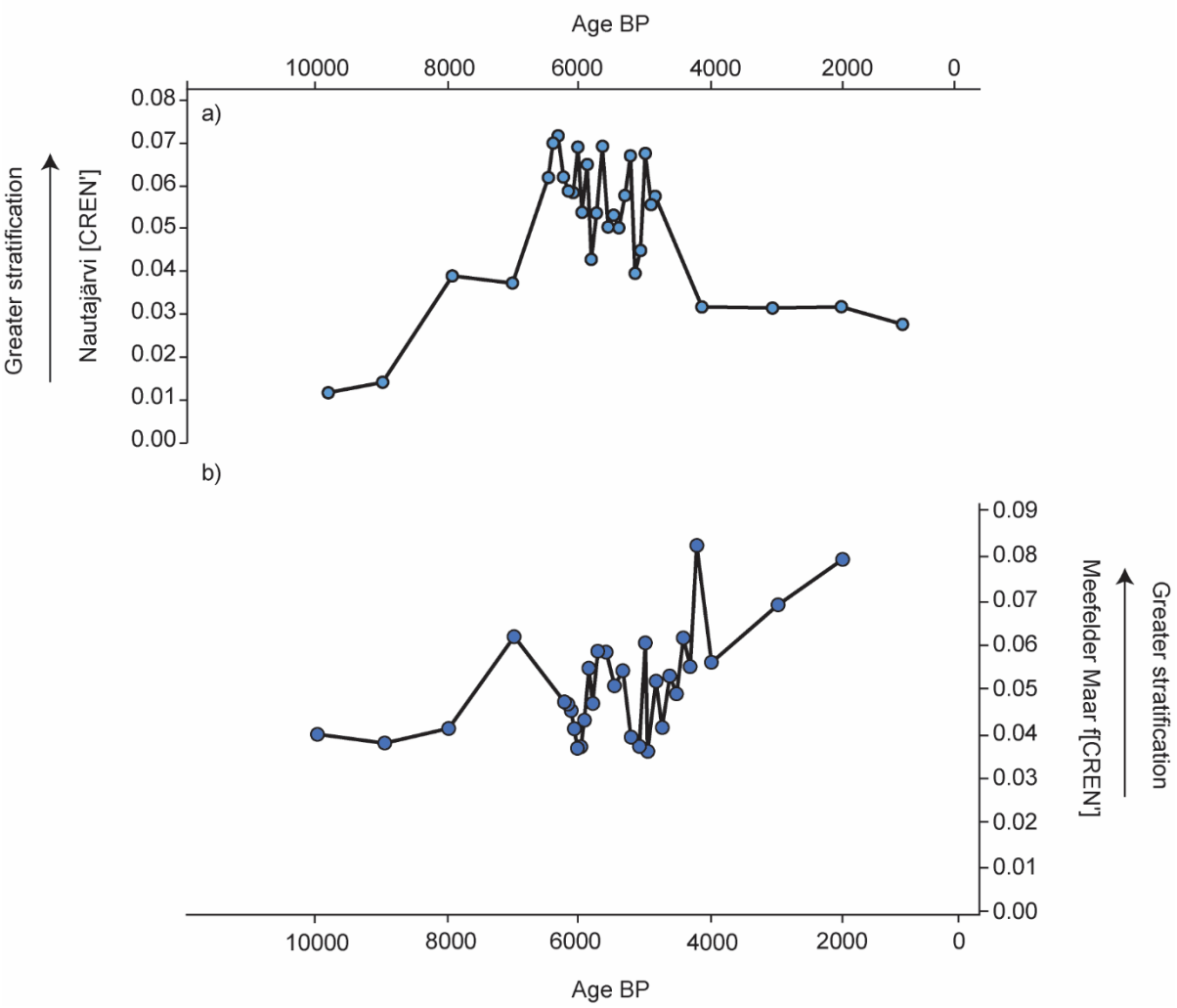

Figure S9. f[CREN'] reconstructions from a) Nautajärvi and b) Meerfelder Maar. Higher values indicate greater stratification.

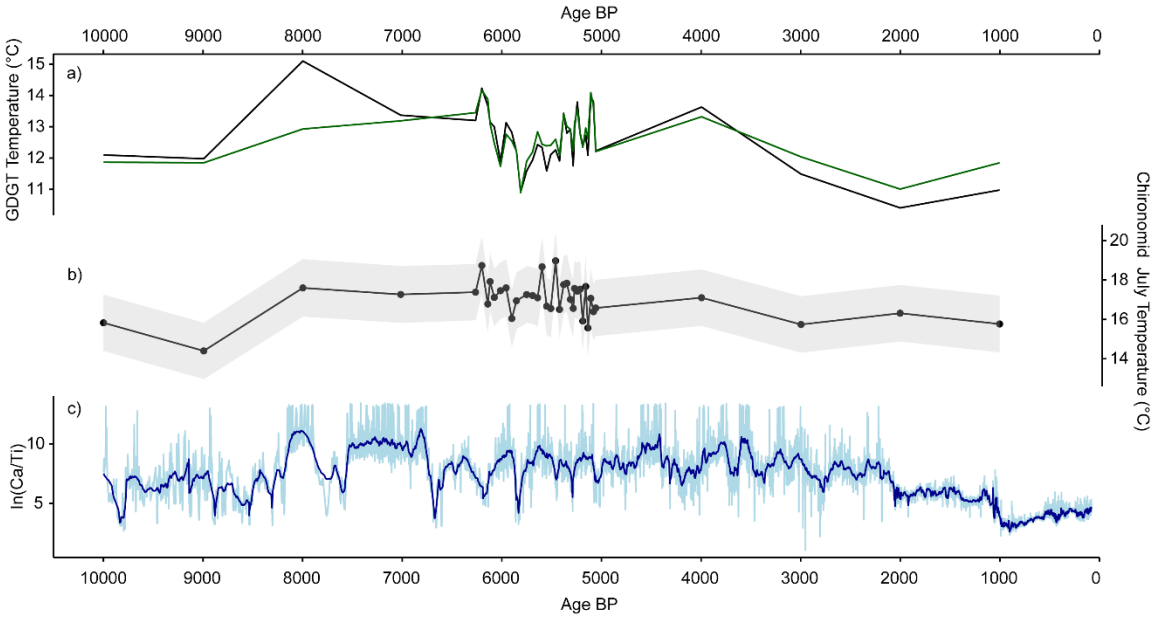

Figure S10. Additional site data from Diss Mere. Shown are GDGT reconstructions from the main body of the manuscript (black, Martinez-Sosa et al., (2021); green, Raberg et al. (2021), chironomid inferred July temperatures (Abrook et al., 2025); and the ln(Ca/Ti) ratio representing variability in summer precipitated calcite and detrital inwash (Boyall et al., 2024).

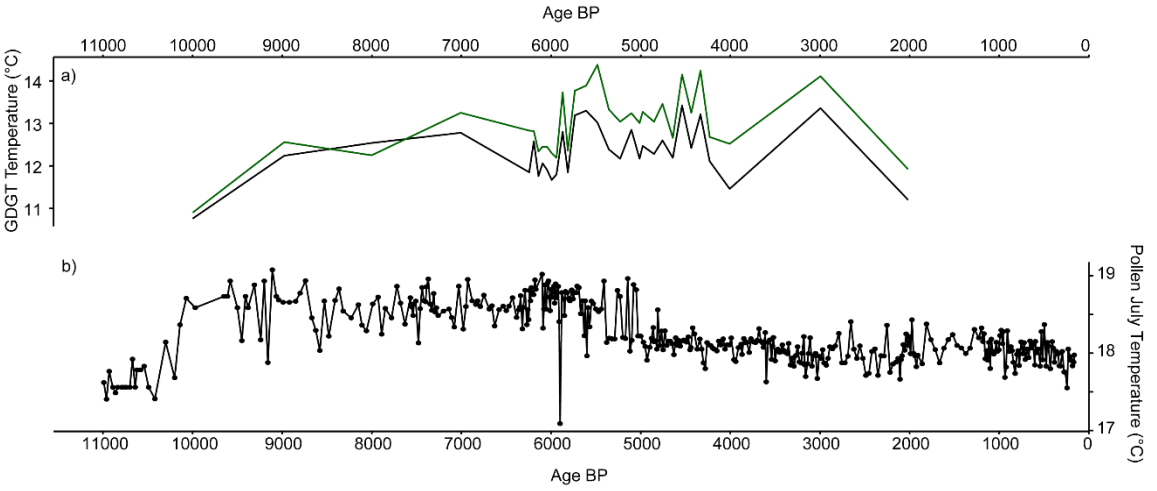

Figure S11. Additional site data from Meerfelder Maar. Shown are a) GDGT reconstructions from the main body of the manuscript (black, Martinez-Sosa et al., (2021); green, Raberg et al. (2021); and b) pollen inferred July Temperatures (Litt et al., 2009).

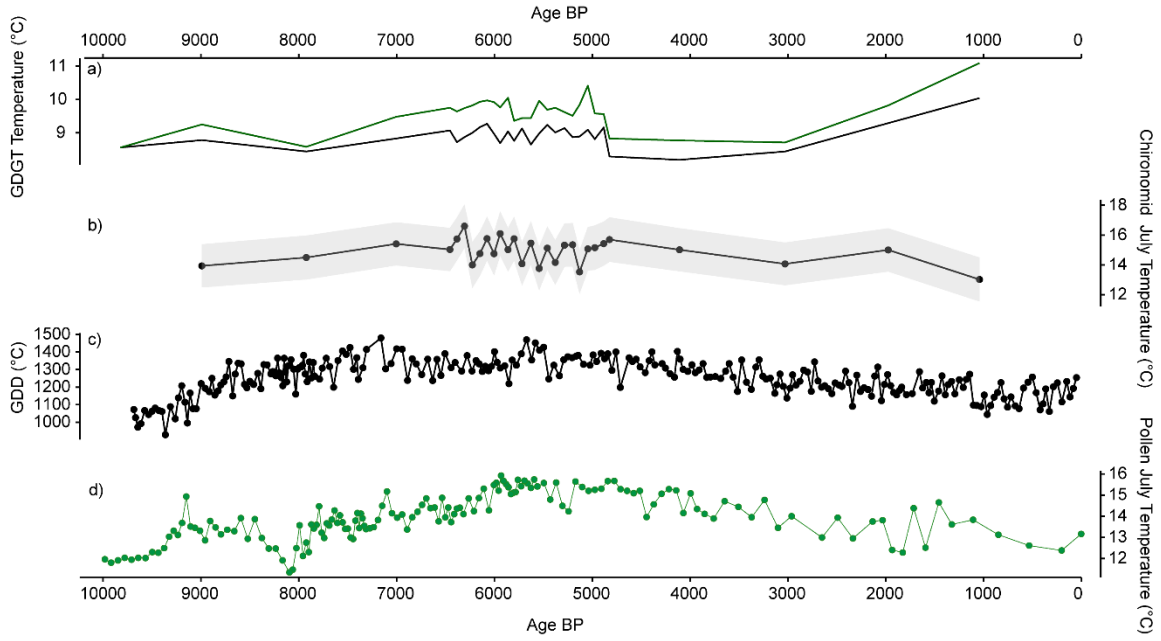

Figure S12. Additional site data from Nautajärvi. Shown are a) GDGT reconstructions from the main body of the manuscript (black, Martinez-Sosa et al., (2021); green, Raberg et al. (2021); b) chironomid inferred July temperatures (Abrook et al., 2025); c) a pollen-based growing degree day (GDD >5 °C) reconstruction (Ojala et al., 2008); and d) a pollen-based reconstruction of July temperatures using a six method ensemble from Lake Kuutsjärvi, Finland (Salonen et al., 2024).

S3. References

Hopmans, E. C., Schouten, S., and Sinninghe Damsté, J. S.: The effect of improved chromatography on GDGT-based palaeoproxies, Org. Geochem., 93, 1–6, https://doi.org/10.1016/j.orggeochem.2015.12.006, 2016.

Litt, T., Schölzel, C., Kühl, N., and Brauer, A.: Vegetation and climate history in the Westeifel Volcanic Field (Germany) during the past 11 000 years based on annually laminated lacustrine maar sediments, *Boreas*, *38*, 4, pp.679-690, https://doi.org/10.1111/j.1502-3885.2009.00096.x, 2009.

Martínez-Sosa, P., Tierney, J. E., Stefanescu, I. C., Crampton-Flood, E. D., Shuman, B. N., and Routson, C.: A global Bayesian temperature calibration for lacustrine brGDGTs, Geochim. Cosmochim. Acta, 305, 87–105, https://doi.org/10.1016/j.gca.2021.04.038, 2021.

Ojala, A.E., Alenius, T., Seppä, H., and Giesecke, T.: Integrated varve and pollenbased temperature reconstruction from Finland: evidence for Holocene seasonal temperature patterns at high latitudes, The Holocene, 18, 4, pp. 529-538, https://doi.org/10.1177/0959683608089207, 2008

Raberg, J. H., Harning, D. J., Crump, S. E., de Wet, G., Blumm, A., Kopf, S., Geirsdóttir, Á., Miller, G. H., and Sepúlveda, J.: Revised fractional abundances and warm-season temperatures substantially improve brGDGT calibrations in lake 935 sediments, Biogeosciences, 18, 3579–3603, https://doi.org/10.5194/bg-18-3579-2021, 2021.

Salonen, J. S., Kuosmanen, N., Alsos, I. G., Heintzman, P. D., Rijal, D. P., Schenk, F., Bogren, F., Luoto, M., Philip, A., Piilo, S., Trasune, L., Väliranta, M., and Helmens, K. F.: Uncovering Holocene climate fluctuations and ancient conifer populations: insights from a high-resolution multi-proxy record from northern Finland, Glob. Planet. Change, 237, 104462, https://doi.org/10.1016/j.gloplacha.2024.104462, 2024.